Excited-State Properties of the Ligand-Localized $^3\pi\pi^*$ State of Cyclometalated Ruthenium(II) Complexes

S. Kimachi, R. Satomi, H. Miki, K. Maeda, and T. Azumi*

Department of Chemistry, Graduate School of Science, Tohoku University, Sendai 980-77, Japan

M. Onishi

Department of Industrial Chemistry, Faculty of Engineering, Nagasaki University, Nagasaki 852, Japan

Received: April 3, 1996; In Final Form: July 8, 1996[⊗]

We report the results of an investigation on the absorption spectra, phosphorescence spectra, phosphorescence lifetimes, and magnetic properties of $[Ru(bhq)(CO)_2Cl(L)]$, where bhq^- is the C-deprotonated forms of benzo[*h*]quinoline (bhqH) and L is either PEt_3, *p*-toluidine, or piperidine. The lowest singlet states of the Ru(II) complexes are metal-to-ligand charge-transfer $^1d\pi^*$ states. Vibrational structures of the phosphorescence spectra observed in the crystalline states at 4.2 K are similar to the structures of the phosphorescence spectra and the magnitude of the free bhqH ligand. Zero-field splittings indicate that the lowest triplet states of all the Ru(II) complexes are mainly characterized as ligand-localized $^3\pi\pi^*$ states. However, the phosphorescence lifetimes are significantly shorter for Ru(II) complexes as compared with free bhqH. This result suggests that the lowest triplet state of the Ru(II) complex includes $^3d\pi^*$ character due to configurational mixing with the bhq-localized $^3\pi\pi^*$ state. By intersystem crossing from the singlet excited state, the in-plane *y* sublevel is the most populated for bhqH, whereas the out-of-plane *x* sublevel is the most populated for the Ru(II) complexes. This dramatic change of the intersystem crossing route is satisfactorily interpreted within the framework of the theory of the intersystem crossing by considering the difference of the character of the lowest singlet state.

1. Introduction

Ru(II) complexes with α,α′-diimine type ligands such as 2,2′-bipyridine (bpy) and 1,10-phenanthroline (phen) have been extensively studied. For example, for $[Ru(bpy)_3]^{2+}$ and $[Ru(phen)_3]^{2+}$, the photophysical and photochemical properties and excited-state dynamics have been well elucidated.[1] The lowest triplet states (T_1) of these Ru(II) complexes are the metal-to-ligand charge-transfer ($^3d\pi^*$) states. Although the T_1's of most of Ru(II) complexes are assigned as $^3d\pi^*$ states, some Ru(II) complexes have T_1's that are characterized with ligand-localized ($^3\pi\pi^*$) states. Available examples[2−4] are $[Ru(i\text{-}biq)_3]^{2+}$ (i-biq = 3,3′-biisoquinoline), $[Ru(bpy)(CNMe)_4]^{2+}$, and protonated $[Ru(bpy)(CN)_4]^{2+}$. However, there has been little research on the $^3\pi\pi^*$ states of Ru(II) complexes. In order to make a detailed analysis, we try to synthesize a series of Ru(II) complexes that have the lowest triplet state of $\pi\pi^*$ nature. In this respect, we focus our attention on cyclometalating ligands, which have strong ligand field strength. When the cyclometalating ligand is coordinated to a metal ion, the $^3d\pi^*$ state should be pushed to higher energy, and therefore, there appears to be a possibility that T_1 is changed from the $^3d\pi^*$ state to the $^3\pi\pi^*$ state. In this paper, we have chosen benzo[*h*]quinoline (bhqH) as the cyclometalating ligand, hoping to obtain the $^3\pi\pi^*$ T_1 state for Ru(II) complexes. We synthesized $[Ru(bhq)(CO)_2Cl(L)]$ (bhqH = benzo[*h*]quinoline; L = PEt_3, *p*-toluidine, and piperidine). For these three complexes, we measured the absorption spectra, phosphorescence spectra, and time-resolved EPR spectra and determined the zero-field splitting (ZFS) parameters and relative intersystem crossing rates, P_i, to sublevels. We then discuss the properties of the T_1's of these Ru(II) complexes. We further discuss the mechanism of the intersystem crossing from the lowest singlet state to the lowest triplet state ($S_1 \rightarrow T_1$ ISC).

2. Experimental Section

Benzo[*h*]quinoline (bhqH) was purified by vacuum sublimation. The syntheses of $[Ru(bhq)(CO)_2Cl(L)]$ (L = PEt_3, *p*-toluidine, and piperidine) were described previously.[5] Good crystals were obtained by a slow diffusion of *n*-hexane to CH_2Cl_2 solution at room temperature for a few days.

Excitation was carried out by the 313-nm line of a 500-W high-pressure Hg lamp, and the phosphorescence spectra were observed with a Spex 1702 monochromator equipped with a Hamamatsu R3896 photomultiplier tube. Phosphorescence decays were measured with excitation by a Molectron UV-24 N_2 laser.

The steady-state EPR experiment was carried out only for free bhqH; for the complexes, steady-state EPR signals were not detected due to short triplet lifetimes. The excitation was carried out by a 500-W Hg lamp through a Toshiba UV-D33S glass filter and a 10-cm-thick water filter. The temperature was maintained at 90 K using a Bruker B-VT 2000 variable-temperature unit.

For time-resolved EPR experiments, a Lumonics EX-600 excimer laser (XeCl, 308 nm) was used as the exciting light source with a repetition rate of 30 Hz. The transient EPR signals were detected by a Bruker ESP 300E spectrometer without field modulation. A PAR Model 162 boxcar averager was used and integrated between 0.5 and 1.0 μs after the laser excitation. The temperature was controlled by an Oxford Model ITC4 temperature controller and an Oxford CF935 continuous He gas flow cryostat for the time-resolved EPR experiments. The steady-state and time-resolved EPR experiments were carried out for ethanol solution at a concentration of 1×10^{-3} M.

3. Results

We assume that the spin axes of free bhqH are the same with those of free phen as shown in Figure 1a. The molecular

[⊗] Abstract published in *Advance ACS Abstracts,* December 15, 1996.

S1089-5639(96)01018-3 CCC: $14.00

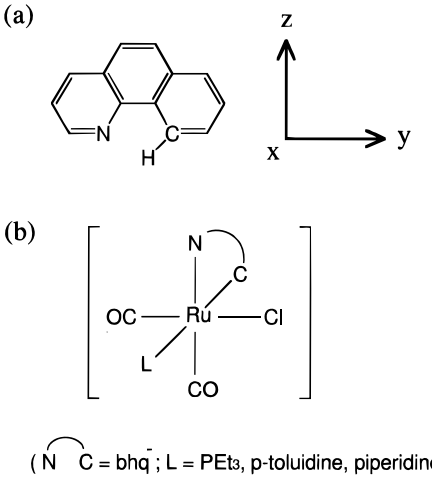

Figure 1. Molecular structures of (a) benzo[*h*]quinoline (bhqH) and (b) [Ru(bhq)(CO)$_2$Cl(L)]. Spin axes of bhqH are also shown.

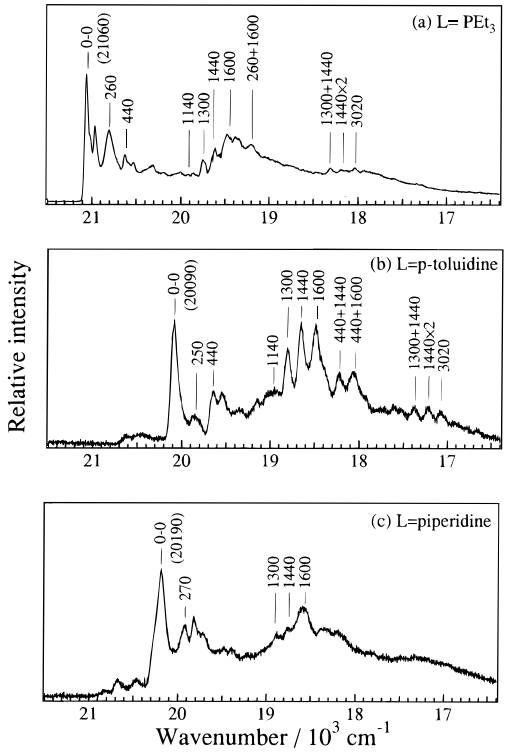

Figure 2. Phosphorescence spectra with vibrational analyses of [Ru(bhq)(CO)$_2$Cl(L)] for (a) L = Pet$_3$, (b) L = *p*-toluidine, and (c) L = piperidine in the crystalline states at 4.2 K.

TABLE 1: Absorption Energy and Assignment of the Lowest Singlet States (S_1) of bhqH and [Ru(bhq)(CO)$_2$Cl(L)] in Ethanol Solution at Room Temperature

sample	E_{abs}/cm^{-1} (ϵ/M^{-1} cm^{-1})	assignment of S_1
bhqH	28 900 (3480)	$^1\pi\pi^*$
L = PEt$_3$	25 760 (2220)	^{1}dπ^*
L = *p*-toluidine	25 480 (3550)	^{1}dπ^*
L = piperidine	25 510 (4290)	^{1}dπ^*

structure of [Ru(bhq)(CO)$_2$Cl(L)] is schematically shown in Figure 1b. This structure was confirmed by NMR and IR spectra.[5]

3-1. Absorption Spectra. The energies and molar extinction coefficients in ethanol solution for bhqH and [Ru(bhq)(CO)$_2$Cl-(L)] are shown in Table 1. For all the Ru(II) complexes, a new absorption band appears at the lower energy region, which is assigned to ^{1}dπ^* (*vide infra*).

TABLE 2: Phosphorescence Lifetimes of bhqH and [Ru(bhq)(CO)$_2$Cl(L)] in Ethanol Glassy Solution at 77 K

sample	lifetime/ms
bhqH[a]	1800[a]
L = PEt$_3$	~42[b]
L = *p*-toluidine	~8[b]
L = piperidine	~8[b]

[a] Methylcyclohexane solvent. [b] Lifetime is not single exponential. The value is the long-lived emission component.

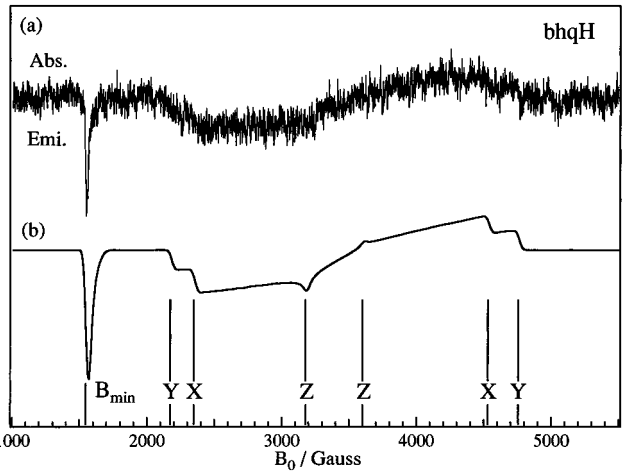

Figure 3. (a) Experimental and (b) simulated time-resolved EPR spectra for T_1 of free bhqH in ethanol glassy solution at 50 K.

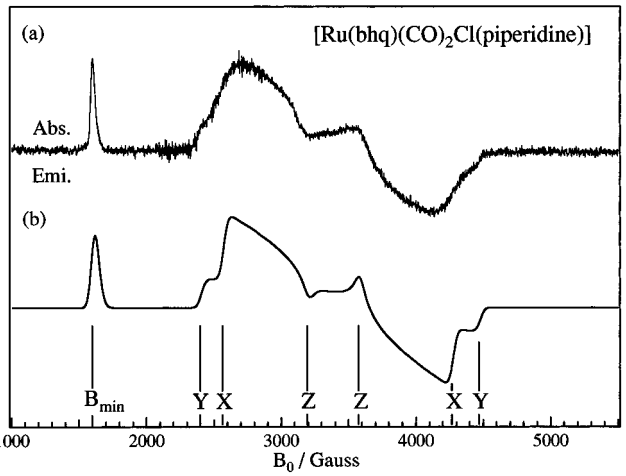

Figure 4. (a) Experimental and (b) simulated time-resolved EPR spectra for T_1 of [Ru(bhq)(CO)$_2$Cl(piperidine)] in ethanol glassy solution at 70 K.

3-2. Phosphorescence Spectra. Well-structured phosphorescence spectra of [Ru(bhq)(CO)$_2$Cl(L)] were observed in the crystalline states at 4.2 K, and the spectra with vibrational analyses are shown in Figure 2.

3-3. Phosphorescence Lifetimes. The phosphorescence lifetimes of the bhqH and Ru(II) complexes observed in ethanol glassy solution at 77 K are shown in Table 2. Significant shortening of the lifetime by coordination to Ru(II) was observed.

3-4. Triplet Sublevel Properties. ZFS parameters of bhqH obtained by steady-state EPR measurements are shown in the top row of Table 3. These values were used for simulation of the time-resolved EPR spectrum of bhqH to obtain the relative populating rates. The time-resolved EPR spectra of bhqH and [Ru(bhq)(CO)$_2$Cl(L)] for L = piperidine are shown in Figure 3 and Figure 4, respectively. Similar spectra were obtained for L = PEt$_3$ and *p*-toluidine, but the spectra are not shown in this

TABLE 3: Zero-Field Energies[a] (cm^{-1}) and Relative Populating Rates to the T_1 Sublevels of Free bhqH and [Ru(bhq)(CO)$_2$Cl(L)]

sample	x	y	z	P_i
bhqH[b]	−0.0673	0.0802	−0.0128	$(P_y - P_x):(P_z - P_x) = 0.80:0.20$
L = PEt_3[c]	−0.055	0.069	−0.013	$(P_x - P_y):(P_z - P_y) = 0.85:0.15$
L = *p*-toluidine[c]	−0.055	0.067	−0.011	$(P_x - P_y):(P_z - P_y) = 0.90:0.10$
L = piperidine[c]	−0.053	0.064	−0.012	$(P_x - P_y):(P_z - P_y) = 0.90:0.10$

[a] $x + y + z = 0$. [b] Steady-state EPR experiment performed at 90 K and time-resolved EPR experiment performed at 50 K. [c] Time-resolved EPR experiment performed at 70 K.

paper. In these figures, B_{min} means the lowest transition field of $\Delta m = \pm 2$, and *X*, *Y*, and *Z* are the canonical resonance fields of $\Delta m = \pm 1$ transitions for randomly oriented samples.[6] *X*, *Y*, and *Z* correspond to the assignment in Figure 1 for bhqH. For [Ru(bhq)(CO)$_2$Cl(L)], we assume that the sublevel order remains unchanged by coordination to the metal. (The shift of the sublevel energies by the second-order spin−orbit coupling is estimated to be less than 0.003 cm^{-1}, and thus, this assumption is reasonable.) The signal at B_{min} is emissive for bhqH and absorptive for all the complexes. This change of the pattern clearly shows that the $S_1 \rightarrow T_1$ ISC process mainly populates the upper sublevel for bhqH and the lower sublevel in the complexes.

The details of the time-resolved EPR results for the bhqH and Ru(II) complexes are shown in Table 3. The ZFS values for the complexes are as small as the values of the free ligand. A remarkable difference for the populating rates is noted between the free ligand and the complexes. That is, for bhqH, the *y* (along the in-plane long axis of bhqH) sublevel is the most populated by $S_1 \rightarrow T_1$ ISC, whereas the *x* (along the out-of-plane axis of bhq^-) sublevel is the most populated for all the Ru(II) complexes.

4. Discussion

4-1. Characterization of the Lowest Singlet State. A new broad absorption band observed at the lower energy region than the first $^1\pi\pi^*$ absorption band of bhqH ligand for the Ru(II) complexes exhibits a red shift in polar solvent, which is characteristic of the charge-transfer state.[5] We thus conclude that S_1 is the $^1d\pi^*$ state for the Ru(II) complexes (see Table 1). This difference of the S_1 character is the main source of the difference in the $S_1 \rightarrow T_1$ ISC processes discussed above.

4-2. Characterization of the Lowest Triplet State. Phosphorescence spectra and the vibrational structures of the Ru(II) complexes are very similar to those of bhqH.[7] For example, the 440-cm^{-1} vibration is assigned to a ring-bending mode, while the 1440- and 1600-cm^{-1} vibrations are assigned to the C═C(N) stretching mode. As for L = PEt_3 and L = piperidine, there is an additional series of bands which are due to a different emitting site. The similarity of the phosphorescence spectra of the Ru(II) complexes in the vibrational structures to the spectrum of bhqH indicates that the T_1 of [Ru(bhq)(CO)$_2$Cl(L)] is characterized as the $^3\pi\pi^*$ state.

The similarity of the ZFS of the bhqH and Ru(II) complexes (Table 3) further supports the above statement that the T_1's of the Ru(II) complexes are mainly the locally excited $^3\pi\pi^*$ states.

The $^3\pi\pi^*$ assignment, however, becomes somewhat questionable if the phosphorescence lifetime data are examined. The shorter lifetime observed for the Ru(II) complexes as compared with bhqH (Table 3) suggests that the T_1 of the Ru(II) complex somewhat includes the $^3d\pi^*$ configuration in a manner similar to the Rh(III) complexes reported previously.[7,8] That is, the wave function of T_1 is expressed as

$$\Psi_{T_1} = a\phi(^3\pi\pi^*) + b\phi(^3d\pi^*) \quad (1)$$

Since the intrinsic phosphorescence lifetime for the $^3d\pi^*$ state is significantly shorter as compared with the $^3\pi\pi^*$ state, even the small mixing coefficient (*b*) affects the observed lifetime to a great extent.

4-3. Mechanism of the $S_1 \rightarrow T_1$ ISC Process. The $S_1 \rightarrow T_1$ ISC of the complexes differs from that of the free bhqH ligand in the following two points. First, significant enhancement of ISC by coordination to Ru is noted. This is understood from the significant shortening of the fluorescence lifetime. (The fluorescence lifetime of bhqH is around 2 ns, and those of complexes are around a few tenths of a nanosecond.[9] Further, the radiative and the nonradiative deactivation to the ground state can be assumed to be little affected by coordination.) The second difference is concerned with the sublevel selectivity. As is shown in Table 3, for the bhqH ligand, the ISC mainly takes place to the *y* sublevel, whereas for the complexes, the ISC to the *x* and *z* sublevels is dominant. In what follows, these dramatic features of the ISC will be discussed based on the theory of ISC.

In the framework of pure spin Born−Oppenheimer basis,[10] the rate constant (k_{ISC}) for ISC from S_1 to the *u* sublevel (u = *x*, *y*, or *z*) of T_1 is expressed as

$$k_{ISC} \propto |(\chi_{S_1,0}\langle S_1|H_{SO}|T_{1u}\rangle|\chi_{T_1,\nu})|^2 \quad (2)$$

where $\chi_{S_1,0}$, $\chi_{T_1,\nu}$, and H_{SO} denote the zero-vibrational wave function of S_1, the ν-vibrational wave function of T_{1u}, and the spin−orbit coupling operator, respectively. The matrix element is then expanded into the Herzberg−Teller series:

$$(\chi_{S_1,0}\langle S_1|H_{SO}|T_{1u}\rangle\chi_{T_1,\nu}) \approx [\langle S_1|H_{SO}|T_{1u}\rangle]_0(\chi_{S_1,0}|\chi_{T_1,\nu}) + \left[\frac{\partial}{\partial Q}\langle S_1|H_{SO}|T_{1u}\rangle\right]_0(\chi_{S_1,0}|Q|\chi_{T_1,\nu}) + \ldots \quad (3)$$

where *Q* means the normal coordinate. Furthermore, the first-order term of this series is expressed as follows:

$$\left[\frac{\partial}{\partial Q}\langle S_1|H_{SO}|T_{1u}\rangle\right]_0 = \sum_m \frac{\langle S_1|H_{SO}|T_{mu}\rangle\langle T_{mu}|H_{vib}|T_{1u}\rangle}{E(T_{1u}) - E(T_{mu})} + \sum_n \frac{\langle S_1|H_{vib}|S_n\rangle\langle S_n|H_{vib}|T_{1u}\rangle}{E(S_1) - E(S_n)} \quad (4)$$

where H_{vib} denotes the vibronic coupling operator.

Following Metz et al.,[11] we consider only the one-center terms of the spin−orbit coupling. In this treatment, the order of the Herzberg−Teller expansion is the most important criterion in considering the sublevel selectivity.[12]

We first analyze the $S_1 \rightarrow T_1$ ISC process for free bhqH. Since the π-electron structure of bhqH should be almost identical to that of phen, we treat the bhq ligand as belonging to the C_{2v} point group.[7] In analogy with phen,[8,13−16] S_1 belongs to $^1A_1(\pi\pi^*)$ and T_1 belongs to $^3B_2(\pi\pi^*)$. The $S_1 \rightarrow T_1$ ISC mechanism for bhqH is shown in Table 4. As is shown in this table, the ISC to the *y* and *z* sublevels is governed by the first-

TABLE 4: Mechanism $S_1 \rightarrow T_1$ Intersystem Crossing for Free bhqH

sublevel	order of Herzberg−Teller expansion	mechanism
T_y	first	$^1A_1(\pi_{a2}\pi_{a2}^*) \xrightarrow{H_{vib}} {}^1A_2(\sigma_{a1}\pi_{a2}^*) \xrightarrow{H_{so}} {}^3B_2(\pi_{b1}\pi_{a2}^*)$
T_z	first	$^1A_1(\pi_{a2}\pi_{a2}^*) \xrightarrow{H_{vib}} {}^1B_1(\sigma_{b2}\pi_{a2}^*) \xrightarrow{H_{SO}} {}^3B_2(\pi_{b1}\pi_{a2}^*)$
T_x		forbidden

TABLE 5: Mechanism $S_1 \rightarrow T_1$ Intersystem Crossing for Ru(II) Complexes

sublevel	order of Herzberg−Teller expansion	mechanism
x	zeroth	$^1A_1(d_{a2}\pi_{a2}^*) \xrightarrow{H_{SO}} {}^3B_2(d_{b1}\pi_{a2}^*) \xrightarrow{IC} {}^3B_2(\pi_{b1}\pi_{a2}^*)$
y	first	$^1A_1(d_{a2}\pi_{a2}^*) \xrightarrow{H_{vib}} {}^1A_2(d_{a1}\pi_{a2}^*) \xrightarrow{H_{SO}} {}^3B_2(d_{b1}\pi_{a2}^*) \xrightarrow{IC} {}^3B_2(\pi_{b1}\pi_{a2}^*)$
z	zeroth	$^1A_1(d_{a2}\pi_{a2}^*) \xrightarrow{H_{SO}} {}^3A_2(d_{a1}\pi_{a2}^*) \xrightarrow{IC} {}^3B_2(\pi_{b1}\pi_{a2}^*)$

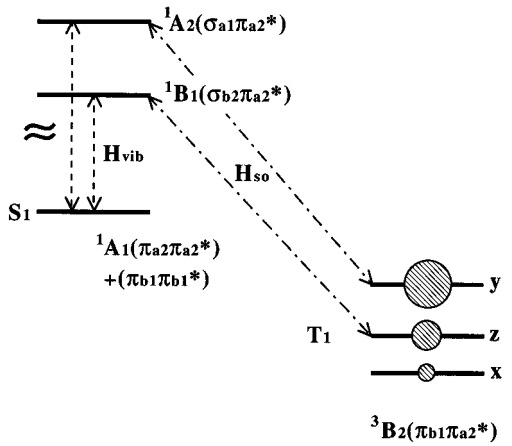

Figure 5. Schematic representation of the mechanism of ISC to triplet sublevels of bhqH. See Table 4 for details.

order term, and in this approximation of considering only the one-center spin−orbit coupling, the ISC to the *x* sublevel is forbidden. The $S_1 \rightarrow T_1$ ISC mechanism for free bhqH is also schematically shown in Figure 5. This theoretical estimation is in good agreement with the experimental results.

We next consider the mechanism for the complexes. For this purpose, we need to know the character of the lowest dπ* singlet state. We can conceive three dπ* states: $^1A_1(d_{a2}\pi_{a2}^*)$, $^1A_2(d_{a1}\pi_{a2}^*)$, and $^1B_2(d_{b1}\pi_{a2}^*)$, which are degenerate in the complexes of cubic symmetry. In the present case, they are no longer degenerate, but it appears that they lie rather closely. Of these three states, the $^1A_1(d_{a2}\pi_{a2}^*)$ state should be more stabilized by the configuration interaction with the $^1A_1(\pi\pi^*)$ state located slightly above it. This configuration interaction picture is also supported from the high-energy shift of the $^1A_1(\pi\pi^*)$ absorption band[5] in the complexes. The other two dπ* states interact only with much highly located $^1\sigma\pi^*$ states, and therefore, the stabilization should be small. Thus, it is reasonable to consider that the lowest singlet state is the $^1A_1(d_{a2}\pi_{a2}^*)$ state.

Below the lowest singlet state, there exist three dπ* triplet states: $^3A_1(d_{a2}\pi_{a2}^*)$, $^3A_2(d_{a1}\pi_{a2}^*)$, and $^3B_2(d_{b1}\pi_{a2}^*)$. The ISC from $^1A_1(d_{a2}\pi_{a2}^*)$ to $^3A_1(d_{a2}\pi_{a2}^*)$ is forbidden, and thus, the ISC's from the lowest singlet state are possible to the remaining two dπ* states. Whichever state is populated by the ISC, it should eventually relax to the lowest triplet state by internal conversion. The mechanism of the ISC for these routes are shown in Table 5.

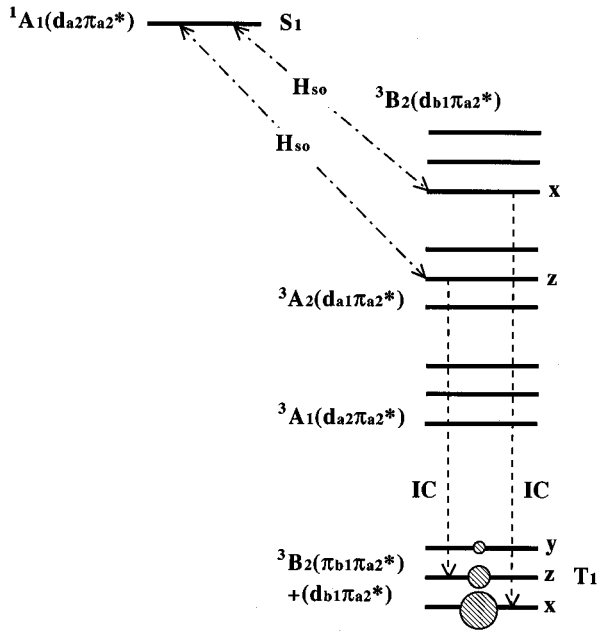

Figure 6. Schematic representation of the mechanism of ISC to triplet sublevels of [Ru(bhq)$(CO)_2$Cl(L)]. See Table 5 for details. IC stands for internal conversion.

As is shown in Table 5, the ISC to the *y* sublevel is allowed only in the first-order term, whereas that to the *x* and *z* sublevels is allowed in the zeroth order. The experimental finding that the *y* sublevel is least populated by ISC is satisfactorily interpreted. Further, all the spin−orbit matrix elements shown in Table 5 involve a one-center term on Rh; this explains the significant enhancement of ISC by complexation.

Acknowledgment. This research was partly supported by a Grant-in-Aid for Development Scientific Research (No. 07554064) and a Grant-in-Aid on Priority-Area-Research on "Photoreaction Dynamics" (No. 07228206) from the Ministry of Education, Science, Sports, and Culture, Japan. We also thank Dr. T. Ikoma for use of the simulation program of time-resolved EPR spectra.

References and Notes

(1) Juris, A.; Balzani, V.; Barigelletti, F.; Campagna, S.; Belser, P.; von Zelewsky, A. *Coord. Chem. Rev.* **1988**, *84*, 85.

(2) (a) Belser, P.; von Zelewsky, A.; Juris, A.; Barigelletti, F.; Tucci, A.; Balzani, V. *Chem. Phys. Lett.* **1982**, *89*, 101. (b) Juris, A.; Barigelletti,

F.; Balzani, V.; Belser, P.; von Zelewsky, A. *Inorg. Chem.* **1985**, *24*, 202. (c) Riesen, H.; Krausz, E. *Chem. Phys. Lett.* **1990**, *172*, 5. (d) Kato, M.; Sasano, K.; Kimura, M.; Yamauchi, S. *Chem. Lett.* **1992**, 1887.

(3) Indelli, M. T.; Bignozzi, C. A.; Marconi, A.; Scandola, F. *J. Am. Chem. Soc.* **1988**, *110*, 7381.

(4) (a) Scandola, F.; Indelli, M. T. *Pure Appl. Chem.* **1988**, *60*, 973. (b) Indelli, M. T.; Bignozzi, C. A.; Marconi, A.; Scandola, F. In *Photochemistry and Photophysics of Coordination Compounds*; Yersin, H., Vogler, A., Eds.; Springer-Verlag: Berlin, 1987; pp 159−164.

(5) Miki, H.; Kimachi, S.; Satomi, R.; Azumi, T.; Onishi, M. *Chem. Phys. Lett.* **1994**, *218*, 563.

(6) (a) Kottis, P.; Lefebvre, R. *J. Chem. Phys.* **1963**, *39*, 393. (b) Kottis, P.; Lefebvre, R. *J. Chem. Phys.* **1964**, *41*, 379. (c) Wasserman, E.; Snyder, L. C.; Yager, W. A. *J. Chem. Phys.* **1964**, *41*, 1763.

(7) Miki, H.; Azumi, T. *J. Phys. Chem.* **1994**, *98*, 6059.

(8) Miki, H.; Shimada, M.; Azumi, T.; Brozik, J. A.; Crosby, G. A. *J. Phys. Chem.* **1993**, *97*, 11175.

(9) Kimachi, S.; Ikeda, S.; Azumi, T. Unpublished data.

(10) Azumi, T. *Chem. Phys. Lett.* **1974**, *25*, 135. Azumi, T.; Matsuzaki, K. *Photochem Photobiol.* **1977**, *25*, 315.

(11) Metz, F.; Friedrich, S.; Hohlneicher, G. *Chem. Phys. Lett.* **1972**, *16*, 353.

(12) Asano, K.; Aita, S.; Azumi, T. *J. Phys. Chem.* **1983**, *87*, 3829.

(13) Komada, Y.; Yamauchi, S.; Hirota, N. *J. Phys. Chem.* **1986**, *90*, 6425.

(14) Gropper, von H.; Dörr, F. *Ber. Bunsen-Ges. Phys. Chem.* **1963**, *67*, 46.

(15) Ohno, T.; Kato, S. *Bull. Chem. Soc. Jpn.* **1974**, *47*, 2953.

(16) Ikeda, S.; Yamamoto, S.; Azumi, T.; Crosby, G. A. *J. Phys. Chem.* **1992**, *96*, 6593.